In vivo detection of basal cell carcinoma: comparison of a reflectance confocal microscope and a multiphoton tomograph

Martina Ulrich
Marisa Klemp
Maxim E. Darvin
Karsten König
Jürgen Lademann
Martina C. Meinke

In vivo detection of basal cell carcinoma: comparison of a reflectance confocal microscope and a multiphoton tomograph

Martina Ulrich,[a] **Marisa Klemp,**[a] **Maxim E. Darvin,**[a] **Karsten König,**[b] **Jürgen Lademann,**[a] **and Martina C. Meinke**[a]
[a]Charité—Universitätsmedizin Berlin, Department of Dermatology, Allergology and Venerology, Charitéplatz 1, 10117 Berlin, Germany
[b]JenLab GmbH, Schillerstr. 1, 07745 Jena, Germany

Abstract. The standard diagnostic procedure for basal cell carcinoma (BCC) is invasive tissue biopsy with time-consuming histological examination. To reduce the number of biopsies, noninvasive optical methods have been developed providing high-resolution skin examination. We present direct comparison of a reflectance confocal microscope (RLSM) and a multiphoton tomograph (MPT) for BCC diagnosis. Both systems are applied to nine patients prior to surgery, and the results are analyzed, including histological results. Both systems prove suitable for detecting typical characteristics of BCC in various stages. The RLSM allows large horizontal overview images to be obtained, enabling the investigator to find the regions of interest quickly, e.g., BCC nests. Elongated cells and palisading structures are easily recognized using both methods. Due to the higher resolution, changes in nucleus diameter or cytoplasm could be visualized with the MPT. Therefore, the nucleus diameter, nucleus/cytoplasm ratio, and cell density are estimated for normal and BCC cells using the MPT. The nucleus of elongated BCC cells is significantly longer than other measured normal skin cells, whereas the cell density and nucleus/cytoplasm ratio of BCC cannot be significantly distinguished from granular cells. © *2013 Society of Photo-Optical Instrumentation Engineers (SPIE)* [DOI: 10.1117/1.JBO.18.6.061229]

Keywords: nucleus diameter; nucleus/cytoplasm ratio; cell density.

Paper 12641SSRR received Sep. 26, 2012; revised manuscript received Jan. 25, 2013; accepted for publication Jan. 29, 2013; published online Mar. 1, 2013.

1 Introduction

Basal cell carcinoma (BCC) represents the most common human skin cancer worldwide, with the incidence steadily increasing among young individuals.[1] BCC mainly occurs on cosmetically sensitive areas of the face or scalp, and early detection and treatment remains crucial to reduce morbidity and improve the cosmetic outcome. Treatment of BCC is usually performed by surgical procedures, including simple excision, Moh's surgery, or reconstructive procedures.[2–4] However, a number of novel noninvasive treatment modalities have become available during the past few decades, which allow for topical treatment of BCC with a good cosmetic outcome. These treatments include topical immunmodulators (e.g., Imiquimod 5% cream) and photodynamic therapy.[5] The standard diagnostic procedure for BCC and other skin cancers is invasive tissue biopsy with subsequent histological examination.[2,3] Histologically, BCCs are characterized by a proliferation of basaloid cells, arranged in nodules of varying size, often connected to the under-surface of the epidermis, and invading the underlying dermis. Tumor nodules show peripheral palisading of cells and nuclei. Different subtypes of BCC can be distinguished, such as nodular, superficial, sclerosing, or infiltrative types, and treatment is guided with regard to the histological classification. The ability to acquire high-resolution images of live tissue would be beneficial, as this would allow for prompt diagnosis of BCC and prevent multiple surgical procedures. Furthermore, early diagnosis would lead to less risk, smaller excisions/scars, and reduced costs for the health care system.

A number of different noninvasive optical methods have been developed in the past few decades. These include reflectance confocal laser scanning microscopy[6] (RLSM), fluorescence laser scanning microscopy[7,8] (FLSM), and multiphoton tomography[9] (MPT). FLSM requires the application of a fluorescent dye, either topically on the skin surface or by intra-epidermal injection. Furthermore, commonly used fluorescent dyes are excited in the blue wavelength range, which has a low penetration depth in the tissue, resulting in a restriction of investigation to the upper 100 μm of the skin. RLSM and MPT typically use near-infrared light for excitation, which has a higher penetration depth in the tissue and can reach the dermis.[10] In the past decade, several groups have shown the applicability of the RLSM method for diagnosis of skin cancer, and instruments for clinical use are currently available.[11–13] Nevertheless, clinical investigations using MPT are now feasible for skin tumor diagnostics.[14] The two methods differ in contrast and resolution because of the different optical interactions. RLSM uses light in the near-infrared range and is based on differences in the refractive index of the tissue or cellular structures. The resolution in RLSM is *typically* 0.5 to 1.0 μm in the lateral direction and 3 to 5 μm in the axial direction, offering the possibility of observing cellular structures down to the upper dermis.

Address all correspondence to: Martina C. Meinke, Charité—Universitätsmedizin Berlin, Department of Dermatology, Allergology and Venerology, Center of Experimental and Applied Cutaneous Physiology, Charitéplatz 1, 10117 Berlin, Germany. Tel: +49 450 518 244; Fax: +49 450 518 918; E-mail: martina.meinke@charite.de

MPT also uses light in the near-infrared range for multi-photon absorption. This is a nonlinear process. There are several endogenous fluorophores in skin tissue, such as oxidated nicotinamide adenine dinucleotide, keratin, melanin, collagen, and elastin, which can be excited by two-photon absorption. The measurement of the autofluorescence is the most commonly used nonlinear process. The resolution is slightly better than for RLSM, i.e., *typically* around 0.5 μm and 1 to 2 μm in the lateral and axial directions, respectively.[9]

Because a system of each method is available in our department, we were able to perform a comparison of the two systems for the measurements of suspected BCC. Successive imaging with RLSM and MPT was followed by correlation with the current "gold standard" of dermatopathology.

Large studies have previously described the RLSM criteria of BCC, including polarized elongated nuclei, linear telangiectasia-like horizontal vessels, basaloid cord and nodules, nests of hyporeflective cells tightly packed in a palisading manner, and horizontal clefting.[6,11,12,14] RLSM exhibits both high sensitivity and specificity for BCC diagnosis.

Preliminary studies have also addressed the MPT criteria for BCC that included jagged cellular contours of keratinocytes, loss of normal cohesion, larger and uneven intercellular spaces, and cells disposed in a random order. Furthermore, elongated nuclei that are monomorphous, polarized, and tightly packed have been described, as well as cells intermingled with fibers (changing laser wavelength from 760 to 800 nm).[14–16]

In this paper, we describe the similarities and differences between the two systems for the diagnosis of BCC, and we refer to the advantages and disadvantages of both techniques with regard to their application in daily clinical routine.

2 Materials and Methods

2.1 Study Participants

The nine patients (three female, six male) who participated in this study were between the ages of 30 and 80, and all had histologically confirmed BCC. Recruitment was performed in the Department of Dermatology, Charité—Universitätsmedizin Berlin, Germany. The BCC lesions were located at the extremities $n = 6$) and on the head $n = 3$). Normal skin areas from all patients served as controls. Unblinded analysis was performed. All research was conducted according to the declaration of Helsinki principles. The study was approved by the local ethical committee at Charité—Universitätsmedizin Berlin, Germany (EA1/046/11), and written informed consent was obtained from each patient prior to enrolment. The patient characteristics are summarized in Table 1.

2.2 Reflectance Laser Scanning Microscope

As a RLSM device, a commercially available system (Vivascope 1500®, MAVIG, Munich, Germany) was used. The system is equipped with an 830-nm low-power diode laser (max. 15 mW, laser class 1M) and a lens with a numerical aperture of 0.9. The device offers a lateral resolution of 0.5 to 1.0 μm and an axial resolution of 3 to 5 μm with a maximum imaging depth of 200 to 250 μm. After the skin was cleaned with an alcohol swab, a drop of immersion oil was applied to the surface of the lesion in order to minimize spherical aberration. Then an objective steel ring with an adhesive plastic ring was applied to the skin. A dermatoscopic image was obtained using an

Table 1 Histologic and clinical data.

Patient	Gender	Age	Location	BCC subtype
1	M	67	Extremity/leg	No subtype
2	M	58	Extremity/leg	Superficial BCC
3	M	71	Extremity/leg	Superficial BCC
4	M	80	Head/forehead	Cystic BCC
5	W	30	Extremity/leg	Superficial BCC
6	W	53	Head/forehead	Superficial BCC
7	M	72	Extremity/leg	No subtype
8	W	80	Head/temple	No subtype
9	M	69	Extremity/leg	Nodular BCC

integrated dermoscopic camera. Subsequently, ultrasound gel was applied between the objective ring and the objective, and the RLSM imaging process was started. Horizontal composite images of 4×4 mm ("confocal mosaics") were obtained on three levels: the stratum corneum, the stratum spinosum, and the superficial dermis. Furthermore, sequential horizontal images of 500×500 μm^2 were obtained on areas of special interest, starting at the stratum corneum and continuing through the stratum granulosum, the stratum spinosum, and the dermal epidermal junction (DEJ) to the superficial dermis. The frame rate was nine frames per second.

2.3 Multiphoton Tomograph

The investigations were carried out with a commercially available two-photon tomograph (JenLab GmbH, Jena, Germany) equipped with a femtosecond titanium sapphire laser (Mai Tai XF, Spectra Physics, USA). The laser was spectrally tunable between 710 and 920 nm and generated 100-fs pulses at a repetition rate of 80 MHz. An excitation wavelength of 760 nm was selected for the investigations. The cellular structure of the skin was investigated at different depths by the autofluorescence and second harmonic generation (SHG) signals,[9,17] which were detected simultaneously by photo multipliers (PMT). High numerical aperture (NA 1.3) piezodriven objective (Zeiss EC Plan-Neofluar $40 \times /1.3$ oil) enables imaging with subcellular spatial resolution. The MPT used offers a lateral and axial resolution of 0.5 and 2 μm, respectively.[18] The typical scan field was 175×175 μm^2, and the frame rate was 13.4 frames per second. For the MPT measurement, a metal ring including a glass window was positioned on the skin after application of a drop of water for an index match. This provided an optical contact between the glass window and the skin. A drop of immersion oil [Immersol (TM) 518F, Zeiss] was applied on top of the glass window, and the oil objective of the MPT was carefully adjusted to the window.

The stratum corneum was identified and denoted as zero. During the measurements, the laser focus was moved from the skin surface in increments of 5 to 10 μm into deeper parts of the skin. The maximum measuring depth into the skin was approximately 200 μm, due to the limited penetration

depth of the laser radiation. During the measurements, the subjects were stabilized using a vacuum pillow to minimize skin movements and to avoid artifacts.

2.4 Study Protocol

The patients were enrolled in the study prior to the planned surgery of clinically or dermoscopically suspected BCC. Written informed consent was obtained prior to enrolment. Investigations of the skin lesions suggestive of BCC and a normal control site were performed by both systems, first with MPT and then with RLSM. Images obtained by both systems were compared with the histological sections obtained from the excised tissue.

2.5 Data Analysis

Analysis of the multiphoton images was performed, including the determination of nucleus diameter, nucleus-to-cytoplasm ratio, and cell density at different depths in normal skin and in BCC. At least six cells from each patient were analyzed using ImageJ (1.45 S). Six to nine subjects were analyzed for each parameter, depending on the quality of the images.

The data were statistically analyzed using SPSS (version 19, Inc. Chicago, Illinois). Because the obtained data were not normally distributed, nonparametric tests were performed. Data were analyzed using the related sample Friedmann's two-way analysis of variances by ranks. Differences among the means were analyzed by the Wilcoxon signed ranks test. Values of $p \leq 0.05$ were considered to indicate a difference.

3 Results

Nine patients were examined using both optical microscopic systems and were analyzed by the typical features described above.

3.1 RLSM

The RLSM device applied in this study offers the additional possibility of obtaining a dermatoscopic image, which can be correlated to the confocal mosaics and therefore allows for orientation within a lesion. Figure 1 shows the dermatoscopic image and the corresponding histological section of a BCC at the lower leg.

Furthermore, large horizontal overview images of up to 8×8 mm in size (total of 256 images) can be performed at any
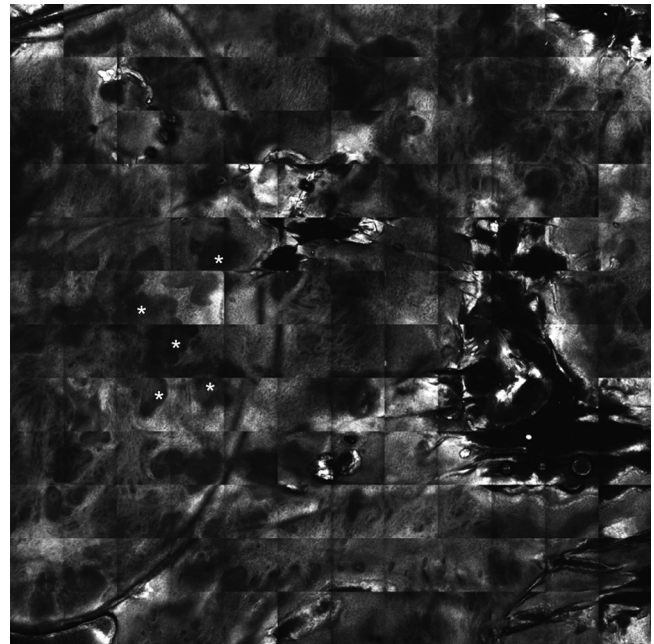
Fig. 2 RLSM overview image (mosaic) of the papillary dermis. Within the mosaic, there are hyporefractile areas that correspond to tumor nests of BCC (red arrows). Furthermore, areas with superficial disruption can be recognized that correspond to surface scales and crusting (white asterisk).

depth (Fig. 2). These mosaics aid in identifying areas of special interest.

Within the analyzed study population, all lesions showed the presence of hyporefractile structures at the level of the DEJ/papillary dermis that corresponds to tumor islands of BCC.

A z-scan can be performed on the regions of interest. In Fig. 3, RLSM images of normal skin and BCC are presented at corresponding imaging depths. Regarding the images of normal skin, cells can be distinguished into granular, spinous, and basal cells. The nucleus appears dark with brighter surroundings, and the diameter of the cells decreases with increasing depth. The cells are arranged in a regular structure. At the basal layer, pigmented cells are visible due to the bright contrast of the melanin and form the bright contours of the papillae at the DEJ. The images obtained for BCC show elongated cells with monomorphic nuclei, hyporefractile areas at the DEJ, and tumor islands of the BCC, which are more pronounced at the deeper levels. The latter shows typical palisading of elongated nuclei and a dark cleft to the surrounding collagen.

3.2 MPT

MPT images of normal skin and a BCC from an area on the same patient are shown in Fig. 4.

The MPT shows horizontal sections of the skin, with the first image showing the cells beyond the stratum corneum. In normal skin, as shown in Fig. 5(a), the cell size decreases as depth increases. The cells have a spherical form in the stratum granulosum and are regularly packed in the stratum spinosum and the basal cell layer. Below 70 μm, the elastin of the upper dermis becomes apparent. In contrast with RLSM, the nuclei are clearly visible, and the cytoplasma of each cell can be clearly distinguished from the surrounding cells, because the cells are surrounded by dark borders.
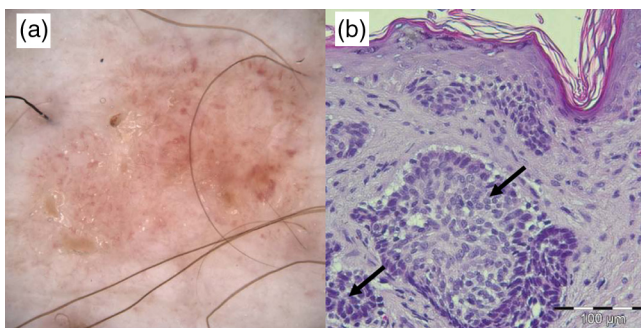

Fig. 1 (a) Dermatoscopic images of a BCC at the lower leg and (b) the histological section of the BCC after surgery with BCC nests (black arrow), Patient No. 1.
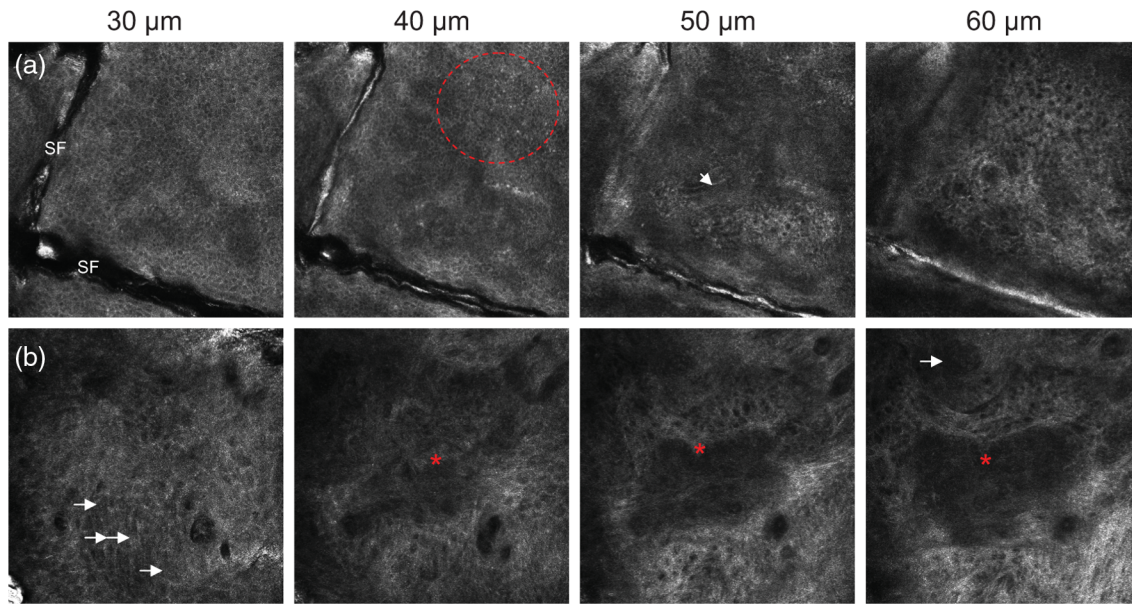
Fig. 3 RLSM images of normal skin (a) and a BCC (b) at different levels in the z-axis of patient 1. (a) At 30 μm, the normal honeycomb appearance of the epidermis can be noted. Furthermore, skin folds are represented by dark lines on RLSM exam. At 40 μm, small bright cells can be observed at the dermo-epidermal junction corresponding to pigmented keratinocytes and melanocytes (red dashed circle). At 50 μm, collagen of the papillary dermis becomes visible, and small blood vessels (white arrow) can be seen. At 60 μm, dermal collagen is visualized. The first image of the BCC (b) shows elongated cells with monomorphic nuclei. At a depth of 40 μm, hyporefractile areas become visible at the DEJ (red asterisk). These indicate the tumor islands of the BCC and become more pronounced at deeper levels. At a depth of 60 μm, a second tumor island becomes apparent that shows the typical palisading of elongated nuclei at the periphery and a dark cleft to the surrounding collagen. The single image size is 500 μm.
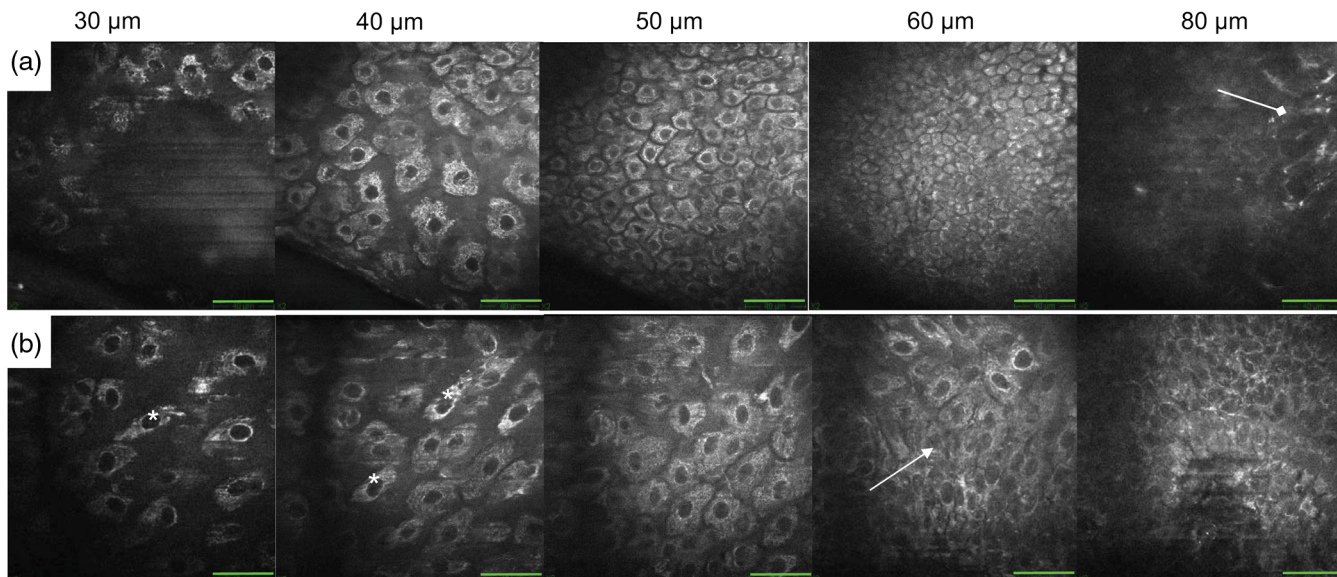

Fig. 4 MPT images at different depths of (a) normal skin and (b) BCC at the lower leg of Patient No. 1. Scale bar = 40 μm. (a) The first granular cells become visible at a depth of 30 μm, the regular honeycomb structure of the stratum spinosum at 50 μm, and the stratum basale at 60 μm. At 80 μm, elastine (arrow) is present. (b) At a depth of 30 and 40 μm, elongated cells with large intercellular distances are visible (asterisk). At 60 μm, palisading of the BCC cells appears (arrow). The cell nuclei become indistinct at 80 μm.

The z-scan through a BCC shows the elongated cells at 30 and 50 μm. In contrast with normal skin, size does not change with increasing depth. In deeper sections, the cell nuclei become indistinct, giving the impression that the cytoplasm is disappearing. The dark borders, which appear between the cells in normal skin at the basal layer [Fig 3(a), 60 μm], are not visible in BCC cells in the deeper sections [Fig 3(b), 80 μm].

In order to develop objective criteria, the nucleus diameter, the nucleus-to-cytoplasm ratio, and the cell density were all estimated for normal and BCC cells.

3.3 Morphological Analysis

The nucleus diameter was determined and is presented in Fig. 5. The nuclei of the granular cells have a significantly bigger
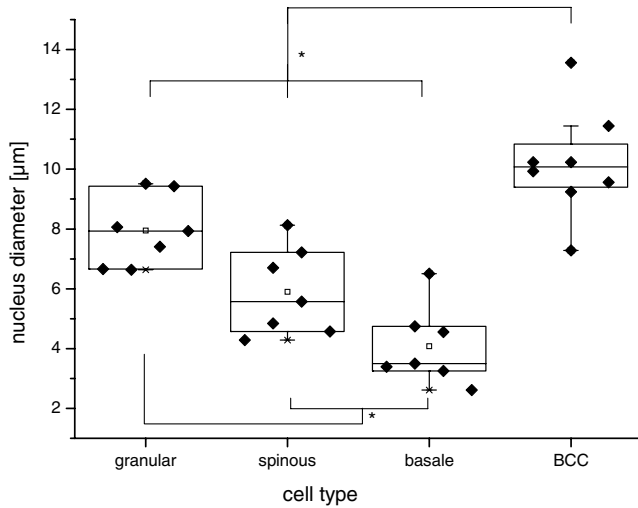
Fig. 5 Nucleus diameter of normal cell types and BCC cells, measured by MPT and analyzed using Image J. At least six cells per patient and cell type were analyzed. *$p < 0.05$.

diameter than spinous and basal cells. Basal cells also have a smaller nucleus diameter than spinous cells $p = 0.107$). The BCC cells have a significantly larger nucleus diameter than all the other investigated cells.

Figure 6 shows the nucleus-to-cytoplasm ratio as box plots for both tissues. The ratio increases with increasing depth. For granular to spinous and basal cells, the differences are significant. The ratio for BCC cells is significantly lower than those of basal and spinous layers. For BCC cells, the mean depth of the ratio determination ranges between 20 and 220 μm (mean 63 ± 50 μm).

The cell density was determined (Fig. 7), showing that the cell density for normal cells increases significantly for granular to basal cells by a factor of 4 and 10, respectively. The cell density in BCC cells is slightly higher than that of the granular layer. The BCC cells were counted in a wide depth range (10 to 200 μm), whereas the granular, spinous, and basal cells were
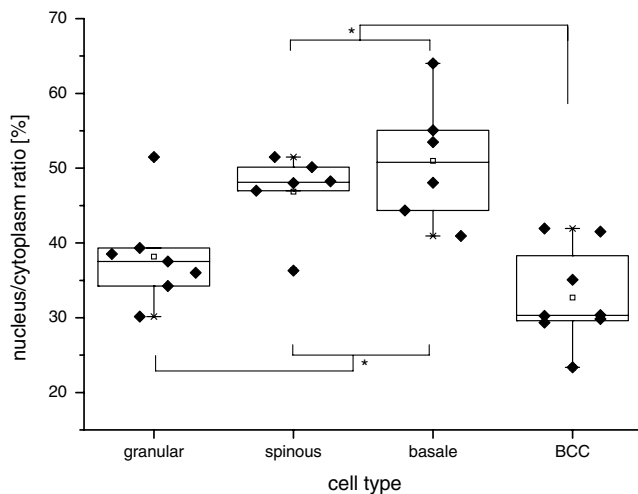

Fig. 6 Box plot of the nucleus-to-cytoplasm ratio of normal and BCC cells. *$p < 0.05$. Normal cells were differentiated in granular, spinous, and basal cell layers; for BCC cells, typical cells were selected at different depths.
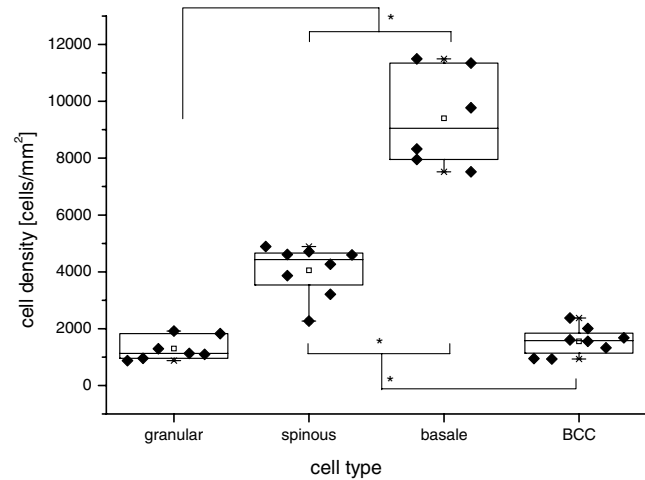

Fig. 7 Cell density of normal and BCC cells measured by MPT and analyzed using Image J. *$p < 0.05$.

counted on average at 21 ± 7 μm, 39 ± 6 μm, and 56 ± 6 μm, respectively.

4 Discussion

Both imaging systems are applicable for the visualization of normal skin and BCC. However, despite the technical differences, several points need to be considered when comparing the two systems. The RLSM device is equipped with a dermoscopy device, which aids navigation within the lesions. Furthermore, a good overview can be obtained by using the composite mosaic image with a maximum size of 8×8 mm. Within a BCC lesion, the characteristic oval or cord-like nest is not uniformly distributed. However, areas of pathologic appearance can be easily identified.

The resolution of the MPT is significantly higher than the RLSM. In contrast to the investigation of Rajadhyaksha et al.[19] using a specially constructed RLSM, the nucleus cannot be so easily differentiated from the cytoplasm in the images obtained in our study. Nevertheless, the decrease in cell diameter in normal skin can be clearly observed. These findings are in agreement with Huzaira et al.[20] using one of the first VivaScopes. Furthermore, the elongated cells, the tumor islands, the typical palisading of elongated cells, and the dark cleft surrounding the collagen are easily visible. The differences in refractive indices are sufficient to distinguish between normal and BCC cell layers, as has been shown in several studies.[6,11,12] The investigation is fast and can be performed in a normal room independent of the surrounding light conditions.

Considering the MPT images, the single cells are clearly visible. This is due to the high amount of NADPH and other fluorophores in the cytoplasm, which gives a bright contrast.

It was possible to estimate the cell diameter of the nucleus and cytoplasm. Therefore, the nucleus-to-cytoplasm ratio could be calculated.

The diameters of the nucleus can be reliably distinguished between normal and BCC cells. The BCC nucleus diameters are significantly larger than those of all the other cells measured in this study. Moreover, the diameter did not change over a wide range of depth. These two criteria could help to differentiate between normal and BCC cells. For normal cells, the nucleus diameters are slightly smaller compared to the findings of

Rajadhyaksha et al., who estimated comparable diameters obtained from histological sections. The mean diameter of 10.2 ± 1.8 μm determined for BCC nuclei, measured by MPT, is higher compared with the findings of de Rosa et al.[21] giving data of 7.29 ± 1.12 μm and 8.54 ± 1.51 μm, whereas the higher value corresponds to the more aggressive type of BCC. The difference could be due to shrinking of the histological section.

The nucleus-to-cytoplasm ratio increases from granular to spinous and basal cell layers as it does for the RLSM, the hematoxylin, and eosin stained sections.[19] In BCC, the ratio is even lower than for the granular cells but is not significant. These values for BCC were achieved, since only the elongated cells, as marked in Fig. 5, were selected for the measurements.

The calculated cell density also increases for normal skin from granular to basal layer, as shown by Rajadhyaksha et al. using RLSM. The absolute values of the MPT evaluation are lower by a factor of 2. This could be due to the fact that only this cell nucleus, which appears in sections 1 to 2 μm thin, could be counted. The resolution of the RLSM is lower (3 to 5 μm), and thin sections for histology are generally 3 to 5 μm thick, so more cells are visible. The cell density of the BCC is comparable to that of the granular layer but did not change over a wide depth range. Also, for cell density, BCC values are obtained from 10 to 200 μm.

Most of the morphologic structure described for BCC in the literature could be confirmed in this study. However, we were unable to observe cell nests in deeper layers (below 120 μm) with MPT, as shown for BCC by Seidenari et al.[15] This can be explained by the inhomogeneous distribution of BCC nests within a lesion and thus the difficulties of finding the right area for MPT image acquisition. Thus, a number of areas should be investigated in order to ensure that BCC cells are not overlooked, especially if the lesion is small. In Table 2, a comparison of the two systems is shown.

Table 2 System comparison using different parameters.

Parameters/imaging systems	RLSM	MPT
Resolution	+	++
Mosaic	++	O
Manageability	++	+
Cytoplasm	+	++
Collagen/elastin	+	++
Polarized elongated features	++	++
Basaloid cord and nodules	++	+
Nucleus diameter	+	++
Linear telangiectasia-like horizontal vessels	++	O
Palisading	++	++
Loss of normal cohesion	+	++
Nests of hyporeflective cells tightly packed in a palisading way	++	+

Finally, it should be mentioned that the MPT also offers measurement of dermal collagen which can be detected by the SHG signal intensity.[22,23]

5 Conclusion

The comparison of the two high-end optical systems has shown that both instruments gave clear images to detect BCC in all investigated patients. The parameters used for diagnosis are partly dissimilar, due to the different optical mechanisms used, and this results in a diverse contrast in the images. Among other morphological cell parameters, the nucleus diameter has been determined by MPT and is significantly larger than normal cells. The RLSM, as used in this study, is more suitable for routine clinical use, whereas the MPT, with its high resolution, is more suitable for research but also has the potential for routine clinical use.

References

1. F. Birch-Johansen et al., "Trends in the incidence of nonmelanoma skin cancer in Denmark 1978-2007: rapid incidence increase among young Danish women," *Int. J. Cancer* **127**(9), 2190–2198 (2010).
2. N. R. Telfer, G. B. Colver, and C. A. Morton, "Guidelines for the management of basal cell carcinoma," *Br. J. Dermatol.* **159**(1), 35–48 (2008).
3. W. Sterry, "Guidelines: the management of basal cell carcinoma," *Eur. J. Dermatol.* **16**(5), 467–475 (2006).
4. H. Breuninger et al., "Brief guidelines: Basal cell carcinoma of the skin," *J. Dtsch. Dermatol. Ges.* **4**(5), 441–443 (2006).
5. M. H. Roozeboom et al., "Overall treatment success after treatment of primary superficial basal cell carcinoma: a systematic review and meta-analysis of randomized and nonrandomized trials," *Br. J. Dermatol.* **167**(4), 733–756 (2012).
6. M. Ulrich et al., "Peritumoral clefting in basal cell carcinoma: correlation of *in vivo* reflectance confocal microscopy and routine histology," *J. Cutan. Pathol.* **38**(2), 190–195 (2011).
7. S. Astner et al., "Clinical applicability of *in vivo* fluorescence confocal microscopy for noninvasive diagnosis and therapeutic monitoring of nonmelanoma skin cancer," *J. Biomed. Opt.* **13**(1), 014003 (2008).
8. V. Czaika et al., "Comparison of transepidermal water loss and laser scanning microscopy measurements to assess their value in the characterization of cutaneous barrier defects," *Skin Pharmacol. Physiol.* **25**(1), 39–46 (2012).
9. K. Konig, "Clinical multiphoton tomography," *J. Biophotonics* **1**(1), 13–23 (2008).
10. A. N. Bashkatov, E. A. Genina, and V. V. Tuchin, "Optical properties of skin, subcutaneous, and muscle tissues: a review," *J. Innov. Opt. Health Sci.* **4**(4), 19 (2011).
11. P. Guitera et al., "*In vivo* confocal microscopy for diagnosis of melanoma and basal cell carcinoma using a two-step method: analysis of 710 consecutive clinically equivocal cases," *J. Invest. Dermatol.* **132**(10), 2386–2394 (2012).
12. S. Nori et al., "Sensitivity and specificity of reflectance-mode confocal microscopy for *in vivo* diagnosis of basal cell carcinoma: a multicenter study," *J. Am. Acad. Dermatol.* **51**(6), 923–930 (2004).
13. S. Ziefle et al., "Confocal laser scanning microscopy vs 3-dimensional histologic imaging in basal cell carcinoma," *Arch. Dermatol.* **146**(8), 843–847 (2010).
14. J. Paoli, M. Smedh, and M. B. Ericson, "Multiphoton laser scanning microscopy–a novel diagnostic method for superficial skin cancers," *Semin. Cutan. Med. Surg.* **28**(3), 190–195 (2009).

15. S. Seidenari et al., "Diagnosis of BCC by multiphoton laser tomography," *Skin Res. Technol.* **19**(1), e297–e304 (2013).
16. S. J. Lin et al., "Discrimination of basal cell carcinoma from normal dermal stroma by quantitative multiphoton imaging," *Opt. Lett.* **31**(18), 2756–2758 (2006).
17. K. Konig et al., "*In vivo* drug screening in human skin using femtosecond laser multiphoton tomography," *Skin Pharmacol. Phys.* **19**(2), 78–88 (2006).
18. K. Konig et al., "Optical skin biopsies by clinical CARS and multiphoton fluorescence/SHG tomography," *Laser Phys. Lett.* **8**(6), 465–468 (2011).
19. M. Rajadhyaksha et al., "*In vivo* confocal scanning laser microscopy of human skin: melanin provides strong contrast," *J. Invest. Dermatol.* **104**(6), 946–952 (1995).
20. M. Huzaira et al., "Topographic variations in normal skin, as viewed by *in vivo* reflectance confocal microscopy," *J. Invest. Dermatol.* **116**(6), 846–852 (2001).
21. G. de Rosa et al., "Comparative morphometric analysis of aggressive and ordinary basal cell carcinoma of the skin," *Cancer* **65**(3), 544–549 (1990).
22. M. E. Darvin et al., "Safety assessment by multiphoton fluorescence/second harmonic generation/hyper-Rayleigh scattering tomography of ZnO nanoparticles used in cosmetic products," *Skin Pharmacol. Physiol.* **25**(4), 219–226 (2012).
23. T. Hompland et al., "Second-harmonic generation in collagen as a potential cancer diagnostic parameter," *J. Biomed. Opt.* **13**(5), 054050 (2008).